In-Plane Elastic Excitations in 1D Polymeric Photonic Structures

W. Cheng,[†] T. Gorishnyy,[§] V. Krikorian,[§] G. Fytas,*[,†,‡] and E. L. Thomas[⊥,§]

Max Planck Institute for Polymer Research, P.O. 3148, 55128 Mainz, Germany; Department of Materials Science and Technology, University of Crete, and FORTH, P.O. 1527, 71110 Heraklion, Greece; Department of Materials Science and Engineering, Massachusetts Institute of Technology, Cambridge, Massachusetts 02139; and Institute for Soldier Nanotechnologies, Massachusetts Institute of Technology, Cambridge, Massachusetts 02139

Received September 11, 2006; Revised Manuscript Received November 3, 2006

ABSTRACT: In-plane phonon propagation in a 1D periodic polymeric film comprised of poly(methyl methacrylate) and poly(ethylene terephthalate) layers was studied using Brillouin light scattering. In contrast to homogeneous-medium-like behavior, five acoustic-like modes with constant phase velocities plus an additional high-frequency localized mode were observed. Finite element analysis was used to compute the theoretical phonon dispersion relation and provide interpretation of the observed propagation modes. Complex features of the phonon dispersion relation were associated with elastic waves propagating within the individual periodic polymer layers. The temperature dependence of sound velocities of these modes was then used to estimate glass transition temperatures of individual nanoscale polymer layers in a sandwiched multilayer assembly.

Introduction

Multilayer polymer films comprised of two or more different polymers often possess superior characteristics, such as improved chemical permeability as well as thermal and mechanical properties, and are widely used in coating and packaging industries. Recently, Weber et al.[1] demonstrated the potential of such films for optical applications by creating broadband omnidirectional dielectric stack mirrors that are based entirely on polymer multilayer architectures. The performance of traditional dielectric stack mirrors made of isotropic materials is limited by Brewster's law, according to which the reflection of p-polarized light at a material interface decreases with increasing angle of incidence and ultimately vanishes at a critical angle (Brewster's angle). In contrast, multilayer mirrors made of highly birefringent polymers can be designed to maintain or even increase reflectivity with increase in incident angle. Each birefringent layer is either uniaxial, with equal in-plane (x, y) refractive indices, or biaxial, with different refractive indices along all three directions (x, y, z). In addition, the in-plane refractive indices of adjacent polymer layers differ, which gives rise to so-called giant birefringent optics accompanied by surprising and useful optical effects.[1]

Currently, great interest is focused on the novel optics of these multilayer mirrors, but much less attention has been paid to their elastic properties. In fact, the giant birefringence of these films is an indication not only of optical anisotropy but also of mechanical anisotropy. The periodic variation of the refractive index along the thickness direction of the film is accompanied by corresponding variation of the elastic constants and layer densities. When the elastic and/or density contrast between adjacent layers is sufficiently large, the film behaves as a one-dimensional (1D) phononic crystal[2−5] with stop bands at certain frequencies for elastic waves propagating along the z direction. On the other hand, waves propagating in the sample plane (xy-plane) are also significantly affected by the elastic properties of individual layers if their wavelengths are comparable to the individual layer thickness h. Consequently, the elastic wave excitations in these multilayer structures carry valuable information about the system, i.e., the elastic properties and the structural periodicity, and are therefore of great importance.[5,6]

High-resolution Brillouin light scattering spectroscopy (BLS) utilizing six-pass tandem Fabry−Perot interferometry, with its noncontact, nondestructive advantages, has proven to be a powerful technique in probing gigahertz frequency phonon excitations (thermally excited elastic waves) in various materials.[6−18] This technique records the spectrum $I(\mathbf{q},\omega)$ of light, which is scattered inelastically by thermal phonons propagating in the sample. Here $\mathbf{q}$ is the scattering wave vector defined by the wave vectors of the incoming and scattered photons as $\mathbf{q} = \boldsymbol{k}_i - \boldsymbol{k}_s$, and ω is the frequency shift of the inelastically scattered light. For homogeneous media, the momentum conservation requires that $\mathbf{q} = \mathbf{k}$, where $\mathbf{k}$ is the wave vector of the acoustic phonon involved in the scattering process. The frequency shift is given by $\omega = \pm ck$ as a result of energy conservation, where c is the phase velocity of the phonon with longitudinal or transverse or mixed polarizations. For inhomogeneous systems with the characteristic spacing $d = O(q^{-1})$, BLS spectra display rich features, such as localized vibration eigenmodes,[7−9] dispersive modes, "Bragg" modes indicative of the structure in phononic crystals,[6,12−14] and Lamb modes in free-standing or supported thin films.[16−18]

In the past BLS has been applied to multilayer thin metal films with the main interest directed to magnetic properties.[19,20] To the best of our knowledge, the only BLS experiment on polymer films with a multilayer structure was performed by Forrest et al.[21] on supported one to five alternating polystyrene/polyisoprene (PS/PI) spin-coated homopolymer thin films. They did not succeed, however, to mechanically resolve the individual homopolymer layers (20−80 nm thick). Instead, their data corresponded to an effective medium behaving like a single component thin film despite the large mechanical contrast between the glassy PS and the rubbery PI at room temperature. Here we report the first BLS experiment on a free-standing polymeric multilayer film. Surprisingly, we resolve up to five acoustic-like in-plane propagating phonons even with $h =$

[†] Max Planck Institute for Polymer Research.
[‡] University of Crete and FORTH.
[§] Department of Materials Science and Engineering, MIT.
[⊥] Institute for Soldier Nanotechnologies, MIT.

10.1021/ma062109i CCC: $33.50
Published on Web 12/19/2006

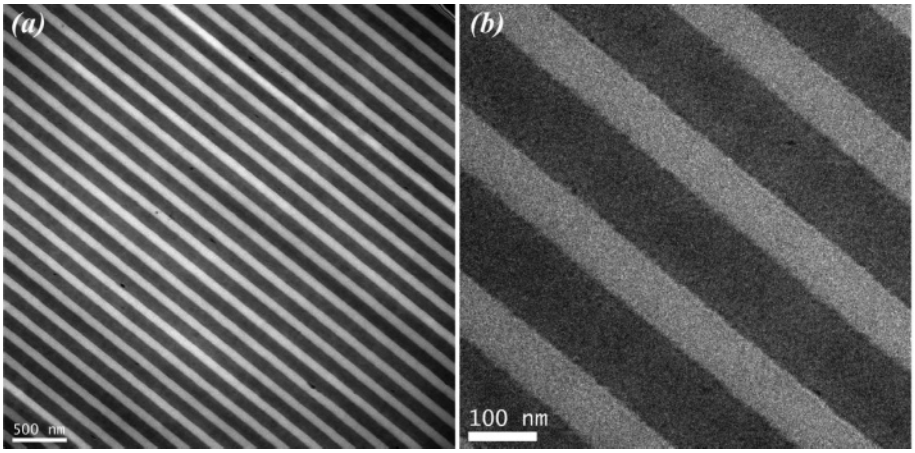

Figure 1. (a) Low- and (b) high-magnification TEM micrographs of PMMA−PET multilayer film; PMMA layer thickness is $h_{PMMA} = 78$ nm and PET layer thickness $h_{PET} = 118$ nm.

$O(q^{-1})$, a condition under which dispersive layer guided phonons are expected.[22] Theoretical dispersion relations computed using finite element analysis (FEA) suggest that these modes are associated with phonons propagating within individual layers. This conclusion is further supported by the measurements of temperature dependence of sound velocities of these modes, which reveal two distinct glass transition temperatures that correspond to phonons localized in poly(methyl methacrylate) (PMMA) and poly(ethylene terephthalate) (PET) layers, respectively.

Experimental Section

Sample. The sample analyzed in this investigation is a multilayer polymer mirror film manufactured by 3M and kindly furnished by A. J. Ouderkirk. The film is a stack of over 200 identical bilayer units composed of 78 nm thick PMMA and 118 nm thick PET layers, as measured by TEM (see Figure 1). PMMA layers are optically and mechanically isotropic, while PET layers possess uniaxial anisotropy with $n_x = n_y \neq n_z$ and $E_x = E_y \neq E_z$. Here n_x, n_y, n_z and E_x, E_y, E_z are refractive indices and Young's moduli along x, y, and z directions, respectively. The degree of birefringence in PET layers was estimated from ellipsometry and polarized reflectometry measurements to be $\Delta n \approx 0.15$. For TEM examination, thin sections of about 60 nm were prepared using a Leica EMUC6 ultra-microtome employing a diamond knife at room temperature. TEM experiments were carried out on a JEOL 2010F equipped with a postcolumn Gatan imaging filter (GIF). The zero loss energy filtered images were taken with an energy window of 15 eV.

Brillouin Light Scattering. The scattering geometry is chosen such that the incident angle α is half of the scattering angle. In this way **q** is parallel to the film plane and its magnitude is independent of the refractive index n, which leads to the equality $q_{||} = q_1 = q_2 = (4\pi/\lambda_0)$ sin α, as shown in Figure 2 for a double-layer film. This also holds for multilayer films. A high-resolution six-pass tandem Fabry−Perot interferometer and a light scattering setup[23] allowing both **q** and temperature variations were employed to record the spontaneous Brillouin spectrum at hypersonic (1−50 GHz) frequencies. Choosing the polarization of the incident laser beam perpendicular (V) to the scattering plane (saggital plane) and selecting the polarization of the scattered light either vertical (V) or parallel to the scattering plane, both polarized (VV) and depolarized (VH) spectra can in principle be recorded. Because of the birefringence of the film, there is a scrambling of the incident and scattered light polarizations, rendering the distinction between the VV and VH spectra ambiguous. Temperature-dependent measurements were done by placing the sample into a heating chamber, and the sample was heated up from room temperature to 140 °C by multiple steps. At every given temperature the sample was stabilized for about 10 min before the beginning of the measurements. Then BLS data were acquired for about 40−60 min for each scan.

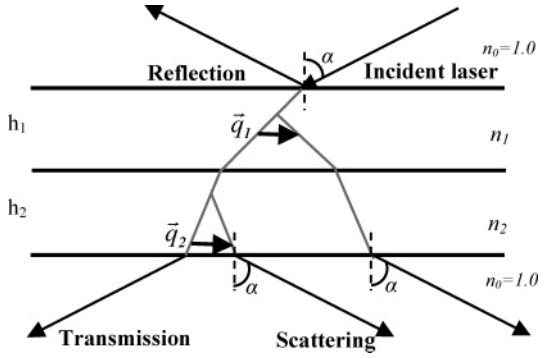

Figure 2. Optical path of the incident laser and the scattered light in a two-layer film with refractive indices n_1 and n_2 for a scattering angle $\theta = 2\alpha$ where α is the angle of incidence.

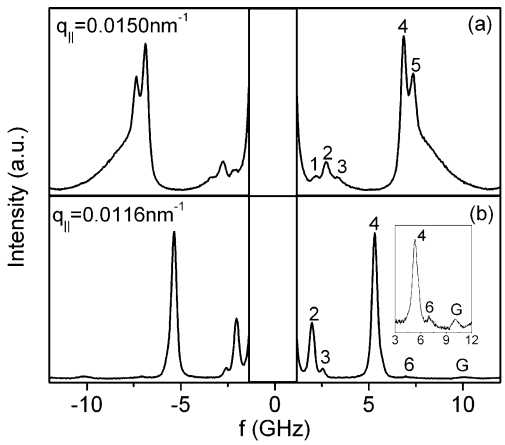

Figure 3. Typical BLS spectra at two different values of the wave vector q at room temperature. The numbers denote the distinct phonons discussed in the text. For clarity, the central Rayleigh line is not shown. The inset plot emphasizes the weak mode (6) by choosing a logarithmic intensity scale. The small feature G is the interferometer ghost of the strong mode (4).

Results and Discussion

Dispersion Relation. Figure 3 shows typical VV Brillouin spectra measured with the $q_{||}$ scattering geometry at two different $q_{||}$ values (0.0116 and 0.0150 nm^{-1}) at ambient conditions. For a better visualization, the central elastic feature due to the reference beam (adopted to stabilize the tandem Fabry−Perot interferometer) was omitted over the frequency range ±1.2 GHz

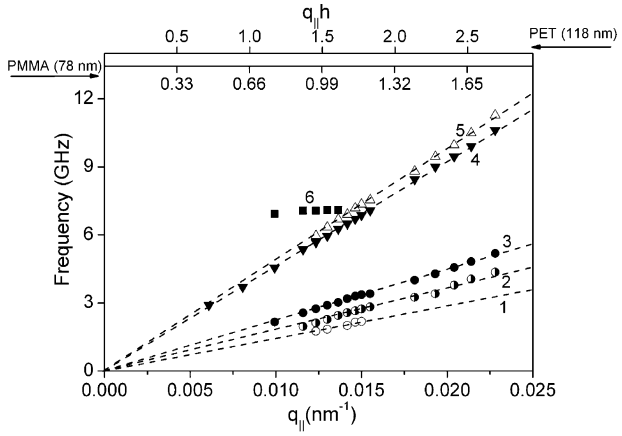

Figure 4. Dispersion relations of the observed elastic excitations in the multilayer film. The dashed lines are the linear fits of the five observed acoustic-like modes; mode 6 is insensitive to $q_{||}$ variations. The upper abscissas show the corresponding $q_{||}h$ ranges for the two constituent layer thicknesses.

around $f = 0$ ($f = \omega/2\pi$). The film displays up to six modes, which are well resolved in the Brillouin spectra of Figure 3a,b. These modes are successively labeled from 1 to 6 in order of increasing frequency. At $q_{||} = 0.0116$ nm^{-1} (Figure 3b), three distinct Brillouin doublets (2−4) are observed, with mode (4) being the most intense. At higher frequencies two additional spectral features (mode (6) and G) can be identified. Albeit barely discernible in the linear intensity scale, their existence is clearly visualized by plotting the intensity logarithmically, as shown in the inset of Figure 3b. The faint peak marked as G is identified as the ghost of the strong mode (4) due to higher order interference effects in the tandem Fabry−Perot interferometer. At higher $q_{||}$ values (Figure 3a) two other modes are resolved: the weak low-frequency mode (1) and the high-frequency mode (5) with intensity comparable to mode (4). Moreover, an additional shoulder-like spectral feature appears on the high-frequency side of mode (5). Note that this shoulder-like spectral feature should not be confused with mode (6) (Figure 3b).

To gain further insight into the physical origin of these modes, we require the dispersion relation, which contains important information about wave propagation by displaying the phonon frequency f experimentally determined as a function of $q_{||}$. To obtain these frequencies f_i ($i = 1-6$), we have represented the BLS spectra by a superposition of up to six Lorentzian line shapes shifted to the observed Brillouin peak positions plus one central line to account for the Rayleigh peak. Figure 4 illustrates the dispersion relation for the in-plane phonon propagation in our polymeric multilayer system. Clearly six modes can be identified and labeled in accordance with the six numbered peaks in Figure 3. At low $q_{||}$ values, due to the proximity of their velocities not all six modes are resolved as is shown in Figure 3b, where merely four modes appear (2−4 and 6). Their identification is based only on the dispersion relation (Figure 4).

These observations are strikingly different from what would be expected if the film (with total thickness of ∼40 μm) behaved as a mechanically homogeneous isotropic medium, where only two bulk modes (longitudinal and transverse) are anticipated. The experimental findings unambiguously suggest the explicit contribution of the individual constituent layers to the elastic excitations of this multilayer film. The result is in clear distinction from the earlier Brillouin study by Forrest et al.,[21] where the dispersion relation of the PS/PI multilayer film was well described by an effective medium approach even though the mechanical contrast between the glassy PS and rubbery PI is large at room temperature.

It is evident from the dispersion relation that five out of six observed modes are strictly acoustic-like. In other words, their frequency increases linearly with $q_{||}$, which results in a constant ($q_{||}$-independent) phase velocity, in clear contrast to surface dispersive modes. According to the two upper abscissas in Figure 4 displaying the $q_{||}h$ values for the two constituent layers, $q_{||}h$ falls roughly between 0.3 and 2.5. In this range, the elastic wavelength and the layer thickness are comparable, and under such conditions, dispersive modes, e.g., Rayleigh, Lamb waves, are expected for either free-standing or supported films.[16−18,21] All these dispersive modes possess both transverse and longitudinal components of the displacement fields, travel parallel to the film surface, and are polarized in the sagittal plane. For supported thin films, the displacement field components decay exponentially into the substrate, confining the mode energy to the near surface region. In our self-supporting polymeric film, except the two outmost layers, every constituent layer A of the same type can be regarded as located in the same microenvironment that is sandwiched by another two identical layers B. For each layer the mechanical boundary conditions encountered are similar to those in supported thin films; thus, similar in-plane phonon propagations with dispersive characteristics are anticipated. The five nondispersive modes showing up in the BLS experiment suggest that we observe other types of phonon propagation in our film. The phase velocities of the five acoustic-like modes are listed in Table 1.

FEA Modeling of the Phonon Dispersion Relation. To provide an interpretation for the observed in-plane propagation modes, we compute the theoretical phonon dispersion relation using finite element analysis (FEA). A two-dimensional (2D) eigenvalue model was created and solved using the COMSOL MULTIPHYSICS 3.2 FEA package based on the linear elastic plain-strain approximation. Since the film is periodic along the z direction, it is sufficient to model a single unit cell consisting of one PMMA and one PET layer and use Bloch boundary condition $\vec{u}(x,0) = \vec{u}(x,d)\exp(iq_z d)$ for the boundaries parallel to the x-axis. Here q_z is the z component of the phonon wave vector and d is the bilayer thickness. The film is homogeneous and infinite (the sample size is much larger than the phonon wavelength) along the x and y directions and the phonon wave vector is taken to be parallel to the x-axis. Thus, we look for the wave equation solution in the form $\vec{u}(x,z) = \vec{u}(z)\exp(iq_x x)$, which leads to the second boundary condition, $\vec{u}(0,z) = \vec{u}(l,z)\exp(iq_x l)$ for the cell boundaries parallel to the z-axis. Here l is a length of the modeling domain along the x direction. This periodicity along the x-axis is artificially introduced in order to apply the FEA, and the solution independent of the actual value of l is used in further analysis. The model meshing and solver accuracy were previously validated by computing phonon dispersion relations for a homogeneous material and for 2D hexagonal phononic crystals and comparing the results with the analytical solutions (homogeneous material) and independent numerical computations (2D phononic crystals).[12,24] In both cases an excellent match was observed.

The amorphous PMMA layer is modeled as an isotropic medium with Young's modulus $E_{\mathrm{PMMA}} = 6.26$ GPa, Poisson ratio $\nu_{\mathrm{PMMA}} = 0.341$, and density $\rho_{\mathrm{PMMA}} = 1200$ kg/m^3. These values for elastic constants are based on independent measurements of the speed of hypersound in pure PMMA films. On the other hand, the PET layer, due to the crystallization ability of PET, has to be taken as anisotropic (uniaxial). Its elastic

Table 1. Elastic Parameters

mode	1	2	3	4	5
sound velocity (m/s)	890 ± 20	1175 ± 23	1415 ± 25	2905 ± 30	3085 ± 30
$(T<T_g) \times 10^4$ (K^{-1})		3.9 ± 0.2	8.6 ± 0.4	9.0 ± 0.4	5.8 ± 0.3
$(T>T_g) \times 10^3$ (K^{-1})		1.46 ± 0.05	1.50 ± 0.06	1.3 ± 0.03	1.23 ± 0.03

constants depend on the degree of anisotropy, which is in turn determined by the history of the sample processing. As a result, it is very difficult to prepare pure PET films with exactly the same elastic constants as in our sample for hypersound velocity measurements. For this reason, we were unable to determine elastic constants of anisotropic PET layers independently and instead used them as fitting parameters to ensure the best match between experimental and theoretical dispersion relation. Rich features of the dispersion relation allow identification of a single combination of elastic constants that provides good agreement between theory and experiment. In particular, we found that the transverse sound velocity was determined almost entirely by shear modulus G_{xz} and the longitudinal sound velocity was influenced primarily by Young's moduli E_x and E_z and Poisson ratios ν_{xy} and ν_{xz}, while the position of the q-independent mode (Figure 4) was a function of shear modulus G_{xz} and Young's moduli E_x and E_z. Accordingly, the PET layer was modeled as a transverse isotropic medium with $E_{x\_PET} = E_{y\_PET} = 6$ GPa, $E_{z\_PET} = 4$ GPa, $\nu_{xy\_PET} = 0.40$, $\nu_{xz\_PET} = 0.48$, $G_{xz\_PET} = 2.2$ GPa, and $\rho_{PET} = 1380$ kg/m^3; here G_{xz_PET} is the shear modulus in the xz plane. These values are consistent with previous studies of elastic constants of anisotropic PET.[25−27]

The theoretical phonon dispersion relation is shown in Figure 5a. For the ease of comparison, experimental data are also plotted on the same graph (black rectangles). Four modes are expected according to the model prediction: a transverse mode (dashed lines), a longitudinal mode (solid lines), and two closely spaced high-frequency quasi-longitudinal guided modes (dotted lines). The details of their displacement fields at $q_{||} = 0.012\,57$ nm^{-1} are shown in Figure 5b−e. Note that for both the longitudinal (Figure 5c) and transverse (Figure 5b) waves the regions of high deformation are not confined to any individual layer, but rather are spread such that their displacement vectors are only weakly dependent on z, especially for the transverse wave. In contrast, for the high-frequency quasi-longitudinal waves there are two regions of high deformation with the displacement vectors antiparallel to each other, as shown in Figure 5d,e. These modes appear as a result of periodicity in the film, and their frequency depends on the film lattice constant. Interestingly, the regions of high displacement of their group velocity are now localized within individual layers.

The positions of all modes are in good quantitative agreement with the experimental data. However, the model does not predict the splitting of the transverse and longitudinal lines into three and two components, respectively, as observed experimentally. It is well-known that optical birefringence or diffraction[28] may lead to the splitting of Brillouin lines due to the possible generation of light beams propagating in directions other than the main beam. However, for the present experiment, these possibilities can be safely ruled out. For $\Delta n = 0.15$, the birefringence induced splitting (ordinary and extraordinary rays) would be an order of magnitude smaller than what we have observed and cannot be resolved experimentally. The small periodicity (compared to the laser wavelength) as well as the weak refractive index contrast also excludes optical diffraction interference, as confirmed by the failure of observing any abnormal optical beams in our experiment. Therefore, we must search for the cause of additional modes within the framework of elastic wave propagation.

There are two relevant length parameters in our problem: the bilayer thickness $d = h_{PMMA} + h_{PET}$ and the phonon wavelength λ. Their ratio $\xi = d/\lambda$ will determine how the propagating waves interact with the layered medium, i.e., if they experience it as a homogeneous medium or if they are sensitive to the structure of the individual layers. The larger ξ, the more we can expect waves to be localized within individual layers. In the extreme case when $\xi \gg 1$, waves propagating in each layer become completely insensitive to the presence of the other layers.

Figure 5b−e shows a weak z dependence for transverse and longitudinal modes, but not for higher frequency q-independent modes. This behavior corresponds to the regime where phonon propagation is starting to be influenced by the multilayer structure of the film. It is helpful then to examine now how the features of the wave propagation change upon further increase in ξ paying special attention to acoustic-like modes. Figure 6 shows the theoretical dispersion relation for the transverse-like (dashed lines) and longitudinal-like (solid lines) modes as well as the extrapolation of the experimental data (dotted lines) based on sound velocities of modes (2)−(5) for $q_{||}$ in the range from 0.05 to 0.07 nm^{-1}. Interestingly, the existence of three transverse-like and three longitudinal-like modes is now predicted by the model. The phase velocities of these modes match the experimental values quite well. Unlike the case of lower q values, the displacements fields of these modes show strong z dependence and are contained either in PET or in PMMA layers. This result suggests that the five acoustic-like modes observed experimentally may come from localized longitudinal-like and transverse-like phonons propagating within individual layers. It is not entirely clear why the theory predicts the line splitting for somewhat higher values of q than observed experimentally. Imperfections at interfaces, such as interfacial roughness and strain fields, as well as certain degree of uncertainty about elastic constants of anisotropic PET layers may be responsible for this difference.

Temperature Dependence of the Elastic Constants. In the previous section, the observed acoustic-like phonons were associated with the individual layers. Since PET and PMMA possess different glass transition temperatures T_g, the variation of the phase velocities of these acoustic-like phonons with temperature is anticipated to display the characteristic kink at T_g, which should occur at distinctly different temperatures. This would be a direct confirmation of their association to the individual layers. In fact, Figure 7, in which the phase velocities of the four modes (modes (2)−(5)) are plotted as a function of T, clearly illustrates that the harder layer (PMMA) exhibits higher T_g (about 100 °C) than the softer layer (PET) with T_g about 80 °C. It is also evident from Figure 7 that modes (2) and (4) should be associated with PET layers and modes (3) and (5) with PMMA layers since they exhibit the same values of T_g, respectively. These results are in accordance with our attempt to associate these modes with the two types of individual layers. The sound velocity of the weak, low-frequency mode (1) shows a very small variation with T that renders the identification of the kink feature ambiguous, and it is therefore excluded from Figure 7.

The dependence of phase velocities of these modes at temperatures above and below T_g can be well described by the linear relation $c(T) = c(0)(1 - \alpha_T T)$ with $c(0)$ being the

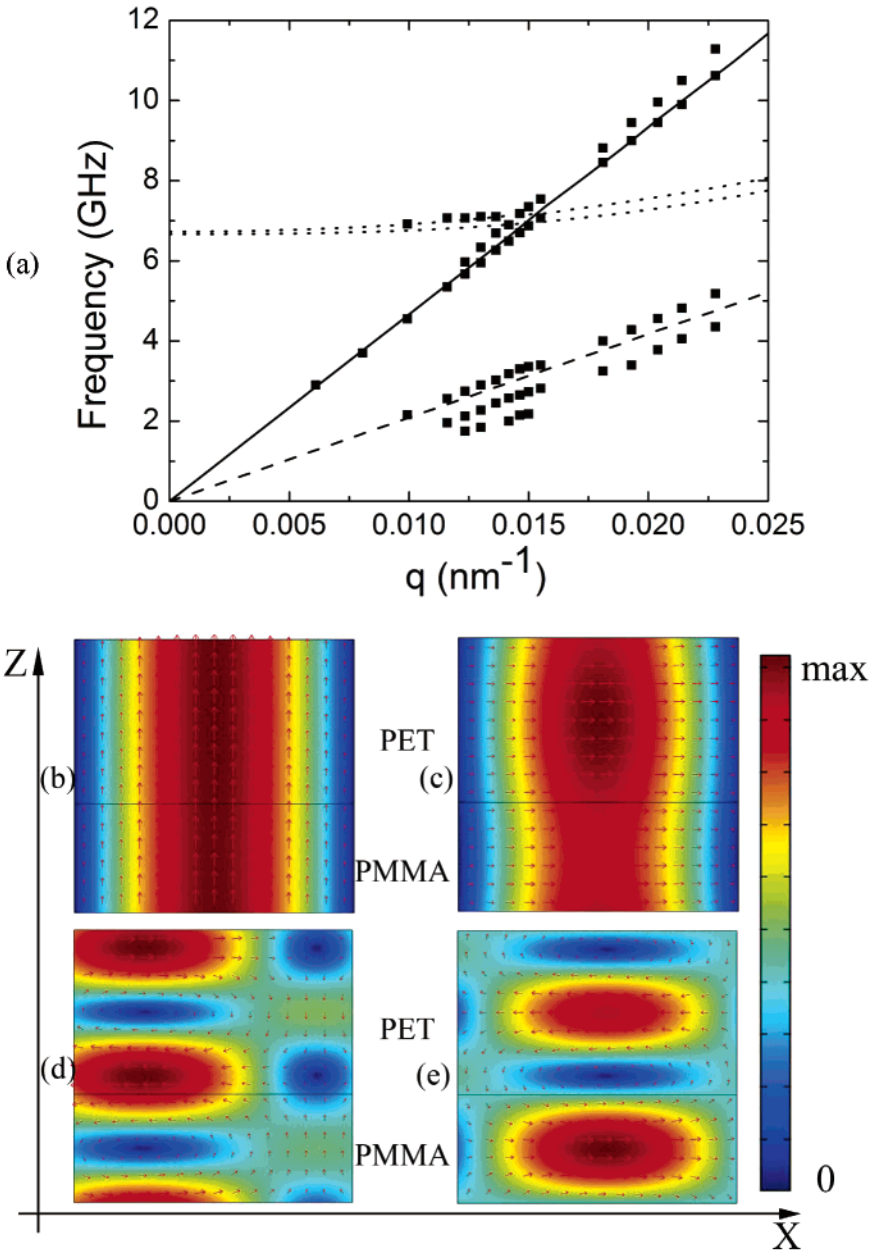

Figure 5. (a) Theoretical phonon dispersion relation and experimental data for the in-plane elastic wave propagation in a multilayer polymer film: solid line, longitudinal mode; dashed line, transverse mode; dotted lines, mixed modes; black rectangles, experimental data. (b) Elastic displacement field for a transverse mode, $k = 0.012\ 57\ \text{nm}^{-1}$. (c) Elastic displacement field for a longitudinal mode, $k = 0.012\ 57\ \text{nm}^{-1}$. (d, e) Elastic displacement fields for mixed antiparallel modes, $k = 0.012\ 57\ \text{nm}^{-1}$.

extrapolated velocity in the particular polymer at 0 K, and α_T is the proportionality coefficient, which describes how rapidly the sound velocity of a particular mode changes with temperature. Since the longitudinal sound velocity is related to the adiabatic compressibility β_s of the material, α_T *of* the two longitudinally featured modes 4 and 5 in different layers characterize the temperature dependence of β_s of the two component materials. In addition, the high-frequency low strain tension/compression and shear moduli are directly determined by the longitudinal and transverse velocities respectively. Therefore, α_T for the four modes also provides the information about the temperature dependence of these two very important material properties, whose values are given in Table 1 for the glassy ($T < T_g$) and the rubbery ($T > T_g$) regimes. These values were obtained by performing a linear fit of experimental sound velocities before and after the glass transition. Data that are in the vicinity of T_g were excluded from the fit. In this context, we should mention that the DSC, a nonlocal technique sensitive to the specific heat change at T_g, was unable to detect the higher T_g, displaying only a single $T_g \sim 75-80$ °C. We recall that the BLS measures the adiabatic compressibility of the system and could, in principle, be utilized to probe the T_g at different layer thicknesses in this sandwiched multilayer arrangement.

For the transverse mode (2) and (3) in the PET and PMMA layer, respectively, the coefficient α_T (Table 1) is somewhat larger than for the longitudinal modes in the rubbery regime. This is expected, since the shear modulus should eventually decrease to zero in the liquid state in contrast to the tension/compression modulus. In the glassy regime, these material properties reflect different deformation of the matter and a prediction on the relative magnitude of α_T for the two moduli is not possible.

Mechanical Anisotropy. The existence of mechanical anisotropy in this polymeric multilayer film is quite probable on the basis of the birefringent nature of the PET layers. Indeed,

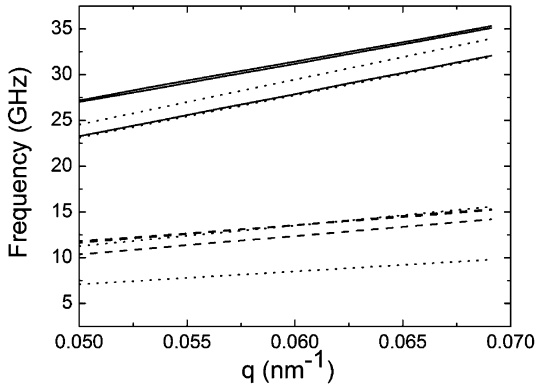

Figure 6. (a) Phonon dispersion relation for $q_{||} = 0.50-0.68$ nm^{-1}: solid lines, theoretical longitudinal modes; dashed lines, theoretical transverse modes; dotted lines, extrapolation of experimental data based on sound velocities for modes (2)−(5).

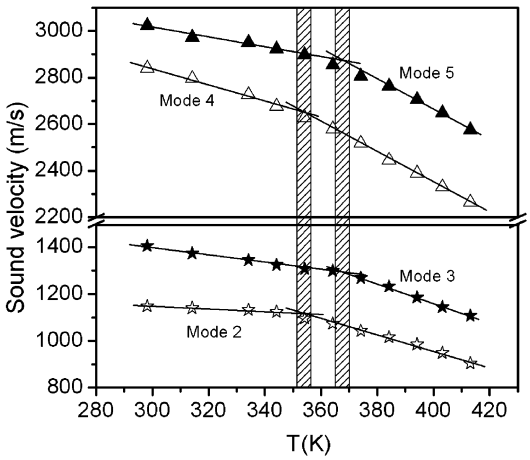

Figure 7. Variation of the phase velocities of the four main modes in the PMMA/PET multilayer film as a function of temperature. The numbers correspond to the mode numbers in Figure 3. The vertical shaded regions denote the region of the respective glass transition temperatures of the two polymers. Solid lines represent the least-square fit to the experimental data before and after the glass transition; data points in the vicinity of T_g were excluded from fitting.

the mechanical anisotropy has already been recognized in the previous modeling of the PET layer in FEA. The reason that the main focus of this work is on phonon propagation parallel to the layers ($q_{||}$) instead of normal to the layers ($q_\perp$) is due to the geometrical restriction that allows to probe only a very narrow range of $q_\perp$. Therefore, it is impossible to record a complete dispersion relation $\omega = \omega(q_\perp)$, as was done for the case of in-plane phonon propagation.

Nonetheless, the mechanical anisotropy can still be revealed with a single measurement at a particular value of $q_\perp$, without having to resort to the dispersion relation. In contrast to the presence of six modes (Figure 3) for the in-plane phonon propagation, only a single longitudinal phonon is resolved in the spectrum of Figure 8 with q perpendicular to the layers. Note that for this scattering geometry (inset to Figure 8) the value of q and hence the phase velocity $c_l = 2\pi f/q$ of the phonon depends on the refractive index n of the film,[29] with larger n leading to larger q. Since $n_{PMMA} = 1.49$ and $n_{PET} = 1.57$ (noncrystalline, isotropic), it is quite safe to assume the lowest limit of n of the film (even after stretching) is 1.5, which gives $q = 0.035$ nm^{-1}.

This q value corresponds to a phonon with a wavelength of about 180 nm, which should be short enough to resolve (180 nm vs 196 nm) the mechanically different two layers. However,

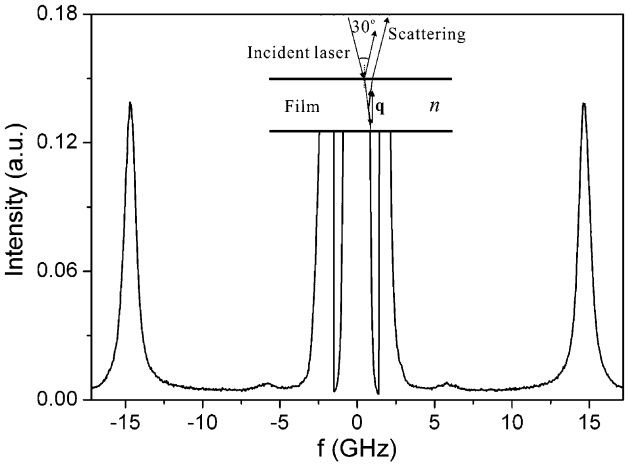

Figure 8. BLS spectrum for the scattering geometry shown in the inset. At the scattering angle 150° and the reflection angle close to 15°, q (=0.035 nm^{-1}) is almost perpendicular to the plane of the film. The peak at about 14.7 GHz corresponds to the longitudinal phonon propagating along the surface normal. The weak feature at about 6 GHz is the ghost of the strong longitudinal peak.

the single phonon spectrum of Figure 8 displaying a longitudinal wave propagating with a phase velocity in an effective medium appears to contradict the layered structure of the film. This apparent contradiction with the in-plane phonon propagation (Figures 3 and 4), where the two layers do exhibit distinct in-plane sound velocities, is easily removed by assuming a sufficiently low elastic contrast between the two layers in the direction of the film normal. For the out-of-plane phonon propagation, we are actually dealing with a 1D phononic crystal. The phononic band structure of this 1D phononic crystal can be calculated by FEA with the use of the same sets of elastic constants for PMMA and PET, which however reveals negligible small Bragg gaps at the first Brillouin zone boundary, $q_\perp = 0.0196$ nm^{-1}. To a good approximation, the phonon propagation along the film normal is isotropic, in accordance with the single experimental phonon spectrum (Figure 8). The experimental and theoretical phase velocities of this single phonon are 2650 and 2580 m/s, respectively. The small difference is not significant considering the uncertainty of the experimental velocity due to the assumption of $n = 1.5$; an increase of n would further narrow this disparity. The absence of the anticipated transverse phonon in the spectrum of Figure 8 is rationalized by the weak elasto-optical coupling at this large scattering angle ($I \sim \cos^2(\theta/2)$, θ is the scattering angle),[30] which leads to very low scattering intensity from transverse waves.

Summary

We report on the features of in-plane phonon propagation in a 1D periodic anisotropic multilayer polymer film. We use BLS to experimentally measure the dispersion relation for gigahertz phonons and find that it is sensitive to the structure of individual layers. Thus, BLS can be used to obtain valuable information about elastic constants of individual layers in nanoscale multilayer assemblies. We observe five acoustic-like propagation modes with constant phase velocities and an additional mode with frequency that is nearly independent of the wave vector. FEA is employed to provide the interpretation for the observed propagation modes. We find that rich features of BLS spectra come from phonons propagating within individual layers and not throughout the whole film as a homogeneous medium. In addition, we study the temperature dependence of sound velocities and show that BLS can be used to estimate glass

transition temperatures of polymer layers with different thicknesses in sandwiched multilayer arrangements. Finally, we show BLS also successfully reveals the mechanical anisotropy of this multilayer film accompanied by its giant birefriengence.

Acknowledgment. We thank Dr. A. J. Ouderkirk of 3M for providing the film. T.G. and E.L.T. thank NSF (Grant 0308133) and ISN of US ARO for financial support.

References and Notes

(1) Weber, M. F.; Stover, C. A.; Gilbert, L. R.; Nevitt, T. J.; Ouderkirk, A. J. *Science* **2000**, *287*, 2451−2456.
(2) Sigalas, M.; Economou, E. N. *Solid State Commun.* **1993**, *86*, 141−143.
(3) Kushwaha, M. S.; Halevi, P.; Dobrzynski, L.; Djafari-Rouhani, B. *Phys. Rev. Lett.* **1993**, *71*, 2022−2025.
(4) Montero de Espinosa, F. R.; Jimenez, E.; Torres, M. *Phys. Rev. Lett.* **1998**, *80*, 1208−1211.
(5) Gorishnyy, T.; Maldovan, M.; Ullal, C.; Thomas, E. L. *Phys. World* **2005**, *18*, 24−29.
(6) Cheng, W.; Wang, J.; Jonas, J.; Fytas, G.; Stefanou, *Nat. Mater.* **2006**, *5*, 830−836.
(7) Kuok, M. H.; Lim, H. S.; Ng, S. C.; Liu, N. N.; Wang, Z. K. *Phys. Rev. Lett.* **2003**, *90*, 255502; **2003**, *91*, 149901 (E).
(8) Cheng, W.; Wang, J. J.; Jonas, U.; Steffen, W.; Fytas, G.; Penciu, R. S.; Economou, E. N. *J. Chem. Phys.* **2005**, *123*, 121104.
(9) Faatz, M.; Cheng, W.; Wegner, G.; Fytas, G.; Penciu, R. S.; Economou, E. N. *Langmuir* **2005**, *21*, 6666−6668.
(10) Priadilova, O.; Cheng, W.; Tommaseo, G.; Steffen, W.; Gutmann, J. S.; Fytas, G. *Macromolecules* **2005**, *38*, 2321−2326.
(11) Hartschuh, R. D.; Kisliuk, A.; Novikov, V.; Sokolov, A. P.; Heyliger, R. R.; Flannery, C. M.; Johnson, W. L.; Soles, C. L.; Wu, W. L. *Appl. Phys. Lett.* **2005**, *87*, 173121.
(12) Gorishnyy, T.; Ullal, C.; Maldovan, M.; Fytas, G.; Thomas, E. L. *Phys. Rev. Lett.* **2005**, *94*, 115501.
(13) Urbas, A. M.; Thomas, E. L.; Kriegs, H.; Fytas, G.; Penciu, R. S.; Economou, L. N. *Phys. Rev. Lett.* **2003**, *90*, 108302.
(14) Tommaseo, G.; Penciu, R. S.; Fytas, G.; Economou, E. N.; Hashimoto, T.; Hadjichristidis, N. *Macromolecules* **2004**, *37*, 5006−5010.
(15) Jang, J. H.; Ullal, C. K.; Gorishnyy, T.; Tsukruk, V. V.; Thomas, E. L. *Nano Lett.* **2006**, *6*, 740.
(16) Sun, L.; Dutcher, J. R.; Giovannini, L.; Nizzoli, F.; Stevens, J. R.; Ord, J. R. *J. Appl. Phys.* **1994**, *75*, 7482−7488.
(17) Grimsditch, M.; Bhadra, R.; Schuller, L. K. *Phys. Rev. Lett.* **1987**, *58*, 1216−1219.
(18) Bandhu, R. S.; Zhang, X.; Sooryakumar, R. Bussmann, K. *Phys. Rev. B* **2004**, *70*, 075409.
(19) D'Orazio, F.; Gubbiotti, G.; Lucari, F.; Tassoni, E. *J. Magn. Magn. Mater.* **2002**, *242*, 535−537.
(20) Giovannini, L.; Donzelli, O.; Ngaboyisonga, J. M. V.; Nizzoli, F.; Carlotti, G.; Gubbiotti, G.; Socino, G.; Pareti, L.; Turilli, G. *J. Magn. Magn. Mater.* **1999**, *199*, 366−368.
(21) Forrest, J. A.; Rowat, A. C.; Kalnoki-Veress, K.; Stevens, J. R.; Dutcher, J. R. *J. Polym. Sci., Part B: Polym. Phys.* **1996**, *34*, 3009−3016.
(22) Farnell, G. W.; Adler, E. L. In *Physical Acoustics, Principles and Methods*; Mason, W. P., Turston, R. N., Eds.; Academic Press: New York, 1972; Vol. 9.
(23) Penciu, R. S.; Kriegs, K.; Petekidis, G.; Fytas, G.; Economou, E. N. *J. Chem. Phys.* **2003**, *118*, 5224−5240.
(24) Maldovan, M.; Thomas, E. L. *Appl. Phys. Lett.* **2006**, *88*, 251907.
(25) Chan, O. K.; Chen, F. C.; Choy, C. L.; Ward, I. M. *J. Phys. D: Appl. Phys.* **1978**, *11*, 617−629.
(26) Feng, R.; Farris, R. J. *J. Appl. Polym. Sci.* **2002**, *86*, 2937−2947.
(27) Anders, S. H.; Eberle, R.; Peetz, L.; Krüger, J.-K.; Göschel, U.; Pietralla, M. *J. Polym. Sci., Part B: Polym. Phys.* **2002**, *40*, 1201−1213.
(28) Cheng, W.; Fytas, G.; Kiyanova, A. V.; Efremov, M.; Nealey, P. F. *Macromol. Rapid Commun.* **2006**, *27*, 702−706.
(29) Tommaseo, G.; Lescanne, M.; Steffen, W.; Fytas, G.; Stamm, M. *J. Polym. Sci., Part B: Polym. Phys.* **2004**, *42*, 3311−3317.
(30) Berne, B. J.; Pecora, R. *Dynamic Light Scattering with Applications to Chemistry, Biology and Physics*; Dover Publications: New York, 1976.

MA062109I